

Quantum Contributions to Free Energy Changes in Fluids

Thomas L. Beck

Departments of Chemistry and Physics
University of Cincinnati
Cincinnati, OH 45221-0172
thomas.beck@uc.edu

To appear in: *Free energy calculations: Theory and applications in chemistry and biology*, Springer-Verlag Press, edited by Andrew Pohorille and Chris Chipot.

Version date May 23, 2005

1.1 Introduction

For the majority of problems in molecular solutions, a classical description is sufficient. In nearly all of the applications discussed so far in this book, that classical limit was assumed in computer simulation calculations of free energy changes. A principal focus is on biological macromolecules such as proteins, and, neglecting any solvent effects for now, those large molecules do not display appreciable quantum effects on their conformational states. Of course internal modes like vibrations are highly quantized, but those modes can typically be treated with rigid constraints or simple classical models due to their small amplitudes of motion. Whatever small quantum effects are present are likely incorporated during empirical fitting of the classical potentials. When should we worry about quantum effects in free energy calculations?

Addressing this question is the subject of this chapter. The emphasis of the chapter is on physical arguments and relatively simple derivations to give a start to somebody interested in checking whether quantum effects should be considered and to provide a set of tools to compute those quantum effects if initial modeling suggests they are important. The approach taken is the path integral formulation of quantum mechanics [1, 2], for two reasons. First, this method gives an intuitive physical picture that adapts naturally to the classical limit: Variational approaches and resulting approximate theories emerge quite easily. Second, the path integral formulation of equilibrium statistical mechanics is well-suited for simulation. The analogy to classical polymer simulations is direct [3], meaning that the quantum simulation merely requires

extending the number of degrees of freedom and employing either Monte Carlo or molecular dynamics procedures to generate the equilibrium distributions. For this reason, the majority of finite-temperature condensed-phase quantum simulations of large systems have utilized path integral methods due to the favorable scaling compared with other quantum methods.

Let's first consider physical systems, in which quantum effects might be important, in the order of decreasing effects. The prototype quantum liquid is liquid helium with its well-known exotic properties. This liquid requires a full quantum treatment and has been examined using path integral simulation [4]. At very low temperatures, particle exchange effects are important in addition to quantum effects due to wavepacket spreading.¹ A second highly quantum example is the solvated electron, which has received a lot of attention from the simulation community [5, 6, 7]. Aside from the interaction of the single electron with atomic cores in the solution modeled with a pseudopotential, exchange effects are not important. Liquid hydrogen is another example with significant quantum effects [8, 9, 10]. Liquids which exhibit quantum effects of smaller magnitude are methane [11, 12], neon [13, 14, 15, 9, 16, 12], and even nitrogen [17]. These moderately quantum systems have been treated successfully with path integral methods and approximations which will be derived in this chapter. Path integral methods have also been applied to compute numerically exact gas phase partition functions for small molecules [18, 19], to predict cluster free energies of formation [20], and to examine quantum effects on melting temperatures for small clusters [20]. In addition, quantum effects on reaction rates in enzymes have received some attention [21, 22]; those models typically employ transition state theory which requires the activation free energy as input. So there has been some work on quantum free energy calculations [23, 24, 25, 26], but much less than for the classical counterpart.

Most of the above systems are prototype 'simple' liquids which require handling of quantum effects. They are foundational in establishing computational methods and approximations, yet they are not of great interest to biological modelers. But liquid water exhibits several interesting quantum effects which are likely to be of some importance for biological molecules in solution. The temperature of maximum density of H₂O is 4°C, while for D₂O it is 7°C higher. The heat of vaporization is 9% larger for D₂O under normal conditions [27]. The solubilities of simple solutes [28] and biomolecules [29] are measurably different in the two liquids, and changes from one solvent to the other can affect protein stability [30]. The triple temperature of H₂O is 4 K lower than that for D₂O, but the critical temperature for H₂O is 3 K higher. And the static dielectric constant for H₂O is higher than that for D₂O by about $\Delta\epsilon \approx 0.35$ [31]. Most of the effects are consistent with a picture of H₂O as a slightly more disordered liquid, which at first glance could be rationalized as a small-mass quantum effect [31]. Since protein conformational states can

¹Indicated by a thermal de Broglie wavelength which is a substantial fraction of the average intermolecular separation.

be quite sensitive to the solvent environment, these effects are large enough to stimulate investigation. Quantum effects can also be expected to contribute significantly to acid-base reactions in water; the structure and dynamics of the proton in water is a subject of intensive current research.

It is interesting that quantum effects in water are not fully understood, and are the topic of current research. This is due to a subtle interplay between several factors influencing water structure and thermodynamics. Classical forcefields have been empirically fit to reproduce a range of structural and thermodynamic experimental data [32]. So these forcefields implicitly incorporate whatever quantum effects might be present. Also, some forcefields do not include intramolecular flexibility or polarizability, factors which may have some importance for the complicated condensed-phase water behavior. Yet when these ‘improvements’ are incorporated, often they lead to worse agreement with experiment. All of these factors lead to a morass of effects which are hard to disentangle. As a first step, if the interest is in quantum effects computed using a realistic empirical potential, the forcefield fitting should be based on a quantum simulation [32].

An even more challenging step has been taken, namely to employ path integral methods for the nuclear degrees of freedom on top of an *ab initio* simulation [33]. As long as a density functional approximation capable of accurately describing water is used for the simulations [34, 35, 36, 37], this approach should yield a good description of the liquid. The calculations are enormously time consuming though; the referenced simulation included 64 water molecules with a total simulation ‘time’ on the order of 15 ps. An issue with this approach is that the path integral description is asked to represent simultaneously both the large intramolecular and small intermolecular² quantum effects on the same footing, creating statistical sampling and perhaps convergence problems [37].

In this chapter it will be suggested that the relatively minor intermolecular quantum effects in a liquid like water are amenable to approximation, and the more quantized intramolecular degrees of freedom can be handled simply say with a normal-mode, harmonic-oscillator picture or even a rigid-molecule representation [37, 38]. Then calculations of free energy changes require only a classical simulation on a modified potential surface.³ The focus will be on free energies, which provide stringent physical tests of forcefields or *ab initio* methods. The excess chemical potential is the natural variable to study for these free energy calculations since it reflects the local environment of a molecule in the solution. The theoretical description of the excess chemical potential stems from the Potential Distribution Theorem [39, 40, 31]. We will see that this description provides a nice route to present the exact quantum

²All degrees of freedom except the intramolecular vibrations.

³That classical calculation may be a density functional theory (DFT) *ab initio* simulation. An *ab initio* treatment may be important to handle charge redistribution effects in the condensed phase.

results with path integral methods, and variational approximations fall out in a few easy steps. The Gibbs free energy is easy to construct once the chemical potentials are obtained: $G = \sum_{\alpha} \mu_{\alpha} n_{\alpha}$, where α labels the chemical species in the solution, μ_{α} is the chemical potential for the species α , and n_{α} is the total number of α molecules.

1.2 Historical Backdrop

A first step towards quantum mechanical approximations for free energy calculations was made by Wigner and Kirkwood. A clear derivation of their method is given by Landau and Lifshitz [41]. They employ a plane-wave expansion to compute approximate canonical partition functions which then generate free energy models. The method produces an expansion of the free energy in powers of \hbar . Here we just quote several of the results of their derivation.

To second order in \hbar the Helmholtz free energy is

$$A \approx A_{\text{cl}} + \frac{\beta^2 \hbar^2}{24} \sum_i \frac{1}{m_i} \langle (\nabla_i U)^2 \rangle_{\text{cl}}, \quad (1.1)$$

where A_{cl} is the classical free energy, $\beta = 1/k_{\text{B}}T$ (k_{B} is Boltzmann's constant and T is the temperature), m_i is the mass of particle i , ∇_i specifies differentiation with respect to the Cartesian coordinates of one of the particles, U is the total system potential energy, and the averaging utilizes classical mechanics. We will see below that several approximation steps are necessary to get to this point, but it follows from the formula that the quantum correction to the classical free energy is positive and related to the average squared forces on the particles. Landau and Lifshitz argue that, under conditions to which the above expansion applies, particle exchange effects appear at third order in \hbar .

By integrating out the coordinate dependence, they also obtain an approximate quantum-corrected formula for the momentum distribution which leads to the definition of an effective temperature. That is, the approximate distribution is still Gaussian in the momenta, but with an increased temperature for each particle:

$$T_{i,\text{eff}} \approx T + \frac{\beta^2 \hbar^2}{12k_{\text{B}}m_i} \langle (\nabla_i U)^2 \rangle_{\text{cl}}, \quad (1.2)$$

which may differ for particles with different masses. This effective temperature suggests that quantum effects can possibly be modeled by simply increasing the temperature in a way related to each particle's mass and the mean square forces on it during its classical motion.

Alternatively, if the momenta are integrated out, an effective distribution of the coordinates is obtained. In this distribution the Boltzmann factor is

sampled with the classical potential energy replaced by a quantum effective potential:

$$U_{\text{eff}} \approx U - \frac{\beta^2 \hbar^2}{24} \sum_i \frac{1}{m_i} (\nabla_i U)^2 + \frac{\beta \hbar^2}{12} \sum_i \frac{1}{m_i} \nabla_i^2 U. \quad (1.3)$$

This potential is similar to one derived by Stratt [42] using different techniques. It is problematic though for simulations of molecular fluids due to the middle term on the right side [12]. The square of the repulsive component of the force leads to unphysical behavior in the effective potential for small separations.

1.3 The Potential Distribution Theorem

A statistical mechanical expression for the chemical potential was derived by Widom in 1963 [39]. His formula is called the Potential Distribution Theorem (PDT). He employed the canonical ensemble, but the PDT can also be derived using a grand canonical approach [31]. The latter derivation leads to a ‘building up’ picture in which the molecule of interest is successively solvated by increasing numbers of surrounding solvent molecules. The resulting expression for the excess chemical potential has the appearance of a partition function formula, but the information required for its evaluation involves only the local neighborhood of the solute. The locality feature distinguishes this picture from the traditional partition function developments. The standard tools of statistical mechanics can be utilized, and often derivations take a particularly simple form when cast in the language of the PDT.

The PDT expression for the chemical potential of a classical molecular species is

$$\beta \mu_\alpha = \ln \left[\frac{\rho_\alpha \Lambda_\alpha^3}{q_\alpha^{\text{int}}} \right] - \ln \langle \langle e^{-\beta \Delta U_\alpha} \rangle \rangle_0. \quad (1.4)$$

The chemical potential μ_α on the left is the full chemical potential including ideal and excess parts. In this chapter we will scale the chemical potentials by β and often refer to this unitless quantity as the chemical potential. $\beta \mu_\alpha$ yields the absolute activity. The first term on the right is the ideal gas chemical potential, where ρ_α is the number density, Λ_α is the de Broglie wavelength, and q_α^{int} is the internal (neglecting translations) partition function for a single molecule without interactions with any other molecules.

The second term on the right is the excess chemical potential resulting from interactions of the distinguished molecule with the surrounding solution. The double brackets indicate averaging over two separate thermal motions, one for the molecule of interest and one for the rest of the system, but with no interactions between the two. Then we take the average of the Boltzmann factor of the interaction energy with the molecule superposed on the solution. This

is an exact expression for the excess chemical potential assuming a classical description is valid.

At equilibrium, the chemical potential for a given molecular species is constant throughout the system. The two terms on the right side of Eq. (1.4) can vary in space, however, so as to add up to a constant: In an inhomogeneous system, the number density and excess chemical potential adjust so as to yield the same constant chemical potential. Due to the local nature of the excess chemical potential, it is reasonable to define an excess chemical potential at a single point in space and/or for a single molecular conformation [31]. That excess chemical potential then determines the local density of the chemical species of interest, once the total chemical potential is specified. This key feature of the PDT permits examination of free energy changes along a specified pathway. An example would be examining free energy profiles along a reaction path in an enzyme [21, 22].

For bookkeeping purposes, it is often easiest to perform the averages in the canonical ensemble. Then the double average for the excess chemical potential can be viewed as follows. The overall distribution to be sampled consists of the Boltzmann factors which contain the potential energies for the N -molecule solution and the internal potential energy for the distinguished molecule. The normalizing factor in the denominator is an integral of this distribution over all coordinates of the solution and the molecule, neglecting the translational degrees of freedom of the molecule.

A useful view of averages can be expressed via the PDT. The configurational average of the quantity F is

$$\langle F \rangle = \frac{\langle \langle e^{-\beta \Delta U_\alpha} F \rangle \rangle_0}{\langle \langle e^{-\beta \Delta U_\alpha} \rangle \rangle_0}. \quad (1.5)$$

The normalization integrals for the averages in the numerator and denominator cancel each other, leaving the traditional expression for the thermal average of F with the distinguished molecule present in the solution. This expression for the average will prove helpful several times below. The PDT is discussed extensively in the chapter by Pratt and Asthagiri, and in Ref. [31].

1.4 Fourier Path Integrals

Feynman, building on earlier ideas of Dirac, developed a formulation of quantum mechanics alternative to the older Heisenberg and Schrödinger pictures [1]. This view expresses the transition amplitude to go from points x to x' in a time t as the superposition of $\exp(iS/\hbar)$ phase factors for an infinite number of paths linking the two points, where S is the action evaluated along the path. When this formulation for real-time evolution is carried over to equilibrium statistical mechanics, the physical time t is replaced by the imaginary time $i\tau$,

where τ ranges from 0 to $\beta\hbar$. This converts the action S to an energy function in a space with an increased number of degrees of freedom specifying the path coordinates for each particle [2]. For all of the systems of interest here, particle exchange effects are negligible, and the paths then are cyclic, starting and ending at the same place. This means that we are assuming Boltzmann statistics. The assumption of Boltzmann statistics is the only approximation required to derive the quantum PDT. The configuration of the whole system then consists of the location of the path origin for each particle and an added set of variables to describe the cyclic paths.

Path integrals can be expressed directly in Cartesian coordinates [1, 2] or can be transformed to Fourier variables [1, 2, 20, 43]. A Fourier path integral method will be used here [20]. The major reason for doing this is that it directly builds length scales into the representation. The Cartesian and Fourier path integrals generate the same physical information, and their mathematical relationship and equivalence have been studied by Coalson [44]. As we will see below, going to a Fourier representation does not involve a Fourier transform operation, but is simply a coordinate change: All of the calculations are still carried out in real space (not \mathbf{k} -space).⁴ At first appearance, the mathematics appears daunting in path integral calculations. But after some exposure to the expressions and practise using them to derive useful results, things begin to look very similar to the more usual classical Boltzmann statistical mechanics. The main purposes in introducing path integrals here are to permit derivation of a quantum version of the PDT and then to obtain useful approximations based on the exact expressions. Those approximations are discussed in the beginning of Section 1.7. After all the path integral gyrations, the Feynman-Hibbs effective potential to model quantum effects turns out to be remarkably simple, namely a Gaussian smear of the potential where the width depends on the temperature and mass.

In what follows, mainly a one-dimensional picture will be employed to avoid a notational proliferation. We will also consider a single *atomic* solute. The methods discussed are easily generalized to three dimensions and many particles: The x, y , and z coordinates of the cyclic path for each atom are represented by a set of Fourier coefficients.

In equilibrium statistical mechanics involving quantum effects, we need to know the density matrix in order to calculate averages of the quantities of interest. This density matrix is the quantum analog of the classical Boltzmann factor. It can be obtained by solving a differential equation very similar to the time-dependent Schrödinger equation:

$$\frac{\partial \rho}{\partial \beta} = -H\rho, \quad (1.6)$$

where ρ is the density matrix and H is the system's Hamiltonian operator. Notice that when you insert the Hamiltonian operator on the right, the equa-

⁴This coordinate change is analogous to changing integration variables x, y, z to spherical polar coordinates r, θ, ϕ .

tion appears quite similar to a diffusion equation. There are many possibilities for solving Eq. (1.6) for ρ ; here we present the path integral representation of the solution.

In coordinate space, the diagonal elements of the canonical density matrix in the Fourier path integral representation are given by [20]

$$\rho(x, x; \beta) = \frac{1}{N!} J(\beta) \int \prod_k da_k \exp\left(-\sum_k \frac{a_k^2}{2\sigma_k^2}\right) \exp\left(-\beta \int_0^1 U[x(\tau)] d\tau\right), \quad (1.7)$$

where the a_k variables are the Fourier coefficients, and, for one particle in one dimension,

$$J(\beta) = \left(\frac{m}{2\pi\beta\hbar^2}\right)^{1/2} \prod_k \frac{1}{\sqrt{2\pi\sigma_k^2}}, \quad (1.8)$$

and

$$\sigma_k^2 = \frac{2\beta\hbar^2}{m(\pi k)^2}. \quad (1.9)$$

$J(\beta)$ is the Jacobian for the transformation from Cartesian to Fourier variables; the Fourier coefficients $\{a_k\}$ used to specify a given path (see below) have the same units as the positional coordinates in the Cartesian path integral. The spreads σ_k in the Gaussian factors in the kinetic energy piece are inversely related to the square roots of the temperature and mass; also, the spreads decrease with increasing Fourier index k . After choosing a position x which is the origin of a given path, then we integrate over all the Fourier variables $\{a_k\}$ to obtain the density matrix element $\rho(x, x; \beta)$. The integral of the potential appearing in the last term involves the fictitious scaled ‘time’ variable τ which ranges from 0 to 1 and expresses the motion along the path. The integrand in Eq. (1.7) is called a *functional*; instead of connecting one variable to another as in a regular function, we need to specify the entire path to return a value for the integrand. We will discuss in more detail the two terms of the integrand below. The integral of Eq. (1.7) over the coordinate x yields the canonical partition function Q .

A path is specified by a set of Fourier coefficients $\{a_k\}$:

$$x(\tau) = x + \sum_k a_k \sin k\pi\tau. \quad (1.10)$$

The location x is the origin of the path, and the Fourier coefficients generate deviations away from that origin. In practical calculations the expansion is truncated at a finite value of $k = k_{\max}$, and the integral of the potential along the path is performed at a discrete set of points chosen fine enough to capture the physical features. It is clear that the high- k modes describe short-wavelength oscillations about the path structure determined by the longer-wavelength, low- k modes. If there are many particles moving in three dimensions, the Jacobian in Eq. (1.8) contains a product over all the masses (with

the exponent 1/2 replaced by 3/2) and over all the Fourier coefficients specifying the paths.

A good example problem is the one-dimensional harmonic oscillator, where $U(x) = m\omega^2 x^2/2$. This case can be solved analytically, and the calculation is fairly lengthy. Here we just quote the results, and encourage the reader to give the derivation a try. To outline the steps, first compute the τ integral of the potential, and then do all of the Gaussian integrals involving the kinetic energy. The result is

$$\rho(x, x; \beta) = C \exp[-S(x, x; \beta)], \quad (1.11)$$

where

$$S(x, x; \beta) = \frac{1}{2}m\omega^2\beta x^2 - \frac{mx^2}{\beta\hbar^2} \sum_k \left(\frac{\beta\hbar\omega}{k\pi} \right)^2 \frac{[1 - (-1)^k]^2}{[1 + (k\pi/\beta\hbar\omega)^2]}. \quad (1.12)$$

Several of the system parameters have been collected in C , which is independent of x . Notice that this result depends on k_{\max} . The analytical result in the $k_{\max} \rightarrow \infty$ limit, obtained by other means in Feynman's book [2], is

$$\rho(x, x; \beta) = C' \exp\left(-\frac{m\omega}{\hbar}x^2 \tanh f\right), \quad (1.13)$$

where C' is another constant and $f = \beta\hbar\omega/2$. We can analyze Eq. 1.13 in the high and low temperature limits. At high temperature, $f \rightarrow 0$ and we can expand the exponentials appearing in the $\tanh f$ term. The result is just the classical distribution for the harmonic oscillator at a given temperature:

$$\rho(x, x; \beta) = C' \exp\left(-\frac{1}{2}m\omega^2 x^2\right). \quad (1.14)$$

At the other extreme of low temperature, $\tanh \rightarrow 1$ and $\rho(x, x; \beta)$ just becomes the square of the ground state wavefunction:

$$\rho(x, x; \beta) = C' \exp\left(-\frac{m\omega}{\hbar}x^2\right). \quad (1.15)$$

What does this example illustrate? First, at high temperatures we know that the paths shrink up due to the decrease in the σ_k values with increasing temperature. Eventually, the paths shrink down to points, and that is the classical limit Eq. 1.14. At the other extreme of low temperature, the paths are more extended since the σ_k values become large, but the potential confines the paths to be distributed in a way that reflects the ground state wavefunction. The approximation methods discussed in this chapter are valid at temperatures where the paths have shrunk to small, but not point-like, sizes.

Given the density matrix, the average of a coordinate-dependent function $F(x)$ is then

$$\langle F \rangle = \frac{\int dx \rho(x, x; \beta) F(x)}{\int dx \rho(x, x; \beta)}. \quad (1.16)$$

This shows that the probability density for the averaging involves a Boltzmann factor which contains a kinetic energy part ($\sum_k a_k^2/2\sigma_k^2$) and the average interaction potential along the path $x(\tau)$. The kinetic energy piece creates an energetic cost when the paths become too extended and/or ‘kinky’, indicated by large values of the Fourier coefficients. The interaction potential is computed only between points with a given τ value and then integrated over τ to get the average; a clear discussion of these points is given in Ref. [13]. This discussion shows that obtaining a quantum average using path integrals is virtually the same as a classical average, except we have to sample in an enlarged space of a_k variables besides the usual positional coordinates x .

Imagine we are using the Metropolis Monte Carlo method to calculate an average. For each trial x and set of Fourier coefficients $\{a_k\}$ during the sampling, we first generate a path and then calculate the kinetic and potential energetic pieces appearing in Eq. (1.7). If this energy in our enlarged space decreases, we accept the trial move; if it increases, we accept with probability proportional to the exponential of the difference of the energy factor between the current and trial configurations in the usual Metropolis way.

If we are interested in the off-diagonal elements of the density matrix, that is $\rho(x, x'; \beta)$, the paths are no longer cyclic but begin at x and terminate at x' . Then the Fourier representation of the path is

$$x(\tau) = x + (x - x')\tau + \sum_k a_k \sin k\pi\tau. \quad (1.17)$$

This picture suggests a trajectory passing from one point to another in a total time $\tau = 1$. For fixed x and x' , we can then imagine sampling those trajectories with a Boltzmann-like weight from an integrand similar to that in Eq. (1.7).⁵ Although the details differ, the transition path sampling method for locating transition states in high-dimensional problems is close in spirit to the path integrals discussed above: Both model a diffusion-like process with fixed endpoints by sampling over a distribution of paths or ‘trajectories.’ This provides an alternative view of boundary conditions for dynamical processes. Instead of producing an ensemble of trajectories with initial positions and momenta, we generate paths which link two points in space in a given time interval. See the chapter by Dellago and the early pioneering work by Pratt [45].

1.5 The Quantum Potential Distribution Theorem

As mentioned above, there are multiple ways to derive the PDT for the chemical potential. Here we utilize the older method in the canonical ensemble which

⁵The energetic factors are slightly more complicated with differing endpoints x and x' .

says that $\beta\mu_\alpha$ is just minus the logarithm of the ratio of two partition functions, one for the system with the distinguished atom or molecule present, and the other for the system with no solute. Using Eq. (1.7) we obtain [46, 47, 9]

$$\boxed{\beta\mu_\alpha = \ln \rho_\alpha \Lambda_\alpha^3 - \ln \left\langle \left\langle e^{-\beta \int_0^1 \Delta U_\alpha[x(\tau)] d\tau} \right\rangle_{a_k} \right\rangle_0}. \quad (1.18)$$

First notice the close similarity to the classical formula for a molecular solute Eq. (1.4). The ideal part of the chemical potential does not contain the internal partition function q_α^{int} since we are considering an atomic solute here. The inner Gaussian average in Eq. (1.18) comes from normalizing factors for the Fourier coefficients in Eq. (1.7). That average pertains to an average over the Boltzmann weight containing the kinetic energy factor alone:

$$\langle \dots \rangle_{a_k} = \frac{\int \prod_k da_k (\dots) e^{-\sum_k \frac{a_k^2}{2\sigma_k^2}}}{\int \prod_k da_k e^{-\sum_k \frac{a_k^2}{2\sigma_k^2}}}, \quad (1.19)$$

that is a Gaussian average with no interactions between the solute and surrounding solvent. The outer average is over the thermal motions of the solvent decoupled from the solute. In place of the interaction energy ΔU_α in Eq. (1.4), we have the average interaction energy along the instantaneous solute path configuration generated during the inner-Gaussian sampling. Eq. (1.18) has been used directly to obtain the excess chemical potential for hydrogen [9] and neon [9, 16] liquids.

We now use a trick to partition this exact expression for the chemical potential into classical and quantum correction parts [31]. To do this we multiply and divide inside the logarithm of the excess term by the classical average:

$$\beta\mu_\alpha = \ln \rho_\alpha \Lambda_\alpha^3 - \ln \left\langle e^{-\beta \Delta U_\alpha(\bar{x})} \right\rangle_0 - \ln \frac{\left\langle \left\langle e^{-\beta \int_0^1 \Delta U_\alpha[x(\tau)] d\tau} \right\rangle_{a_k} \right\rangle_0}{\left\langle \left\langle e^{-\beta \Delta U_\alpha(\bar{x})} \right\rangle_{a_k} \right\rangle_0}. \quad (1.20)$$

The Fourier coefficient average in the denominator of the last term is added to make the numerator and denominator symmetrical. It has no effect on the classical average. The classical factor $\Delta U_\alpha(\bar{x})$ signifies that the potential is evaluated at the centroid of the path:

$$\bar{x} = \int_0^1 x(\tau) d\tau = x + \frac{1}{\pi} \sum_k \frac{a_k}{k} [1 - (-1)^k]. \quad (1.21)$$

This is helpful in deriving approximations later. Intuitively it makes sense since we would like to evaluate fluctuations about the ‘center-of-mass’ of the path.

In the numerator of the last term, we then multiply and divide by $\exp(-\beta\Delta U_\alpha(\bar{x}))$, which means adding and subtracting $-\beta\Delta U_\alpha(\bar{x})$ inside the exponent. This puts the term in the form of Eq. (1.5), where F is everything left over besides the $\exp(-\beta\Delta U_\alpha(\bar{x}))$ factor. We can finally write the quantum PDT as

$$\beta\mu_\alpha = \ln \rho_\alpha \Lambda_\alpha^3 - \ln \left\langle e^{-\beta\Delta U_\alpha(\bar{x})} \right\rangle_0 - \ln \left\langle \left\langle e^{-\beta \int_0^1 [\Delta U_\alpha[x(\tau)] - \Delta U_\alpha(\bar{x})] d\tau} \right\rangle_{a_k} \right\rangle_{\text{cl}} . \quad (1.22)$$

The first two terms on the right are the classical chemical potential, and the last term is an *exact* quantum correction. The averaging in that last term is over the Gaussian kinetic energy piece and the cl subscript on the outer average now says that the *classical* solute is included during the calculation; the average is over the classical reference system. This partitioning is fruitful in deriving approximations for the quantum correction to the excess chemical potential. The inclusion of the classical solute during the averaging process makes the calculation less noisy than the brute force approach suggested by Eq. (1.18).

1.6 Variational Approach to Approximations

The calculation of the quantum correction to the excess chemical potential is of the form

$$-\ln \langle e^{-\beta f} \rangle_{a_k} . \quad (1.23)$$

We will consider expression (1.23) as a schematic for the inner a_k averaging in Eq. (1.22). Let's now explore an approximation for this expression. First, expand the exponential and take the averages of the terms in increasing powers of β . We'll consider terms here up to second order in β . Then, expand the logarithm and we get

$$-\ln \langle e^{-\beta f} \rangle_{a_k} \approx \beta \langle f \rangle_{a_k} - \frac{\beta^2}{2} [\langle f^2 \rangle_{a_k} - \langle f \rangle_{a_k}^2] + \dots \quad (1.24)$$

These are the first two terms in a cumulant expansion [48].

An inequality then proves useful [2]:

$$\langle e^{-\beta f} \rangle_{a_k} \geq e^{-\beta \langle f \rangle_{a_k}} . \quad (1.25)$$

This inequality is called the Gibbs-Bogoliubov-Feynman bound [49], and it can be obtained as the instantaneous-switching limit of Jarzynski's theorem relating nonequilibrium trajectories to free energy changes.⁶ It says that if we

⁶See discussion of Jarzynski's theorem in Chapter ?

just retain the first-order term in β , the approximated quantum correction lies above the exact quantum result. The second-order term is always negative, which also gives an indication that the exact result lies below the approximate one. In addition, the classical free energy lies below the exact quantum result [50, 43, 51]. Thus the exact quantum free energy is bounded above and below by values that can be obtained using classical mechanics for the sampling. This useful point does not seem to have been exploited much in computations of free energies.

1.7 The Feynman-Hibbs Variational Method

The physical principle underlying the following approximations is that relatively weak quantum effects are reflected in narrow Gaussian distributions in Eq. (1.19). The small widths are due to large mass and high temperature. This means that the potential does not vary much over the length scales sampled by the kinetic energy distribution. Additionally, the higher- k Fourier modes become successively narrower. This length-scale argument was invoked in the development of the partial averaging method by Doll and coworkers [20]. In this method, the equality in (1.25) is employed to obtain an effective potential along the path specified by the long-wavelength modes. That effective potential involves a Gaussian smear of the potential with a width determined by the largest chosen $k = k_{\max}$. The effective potential allows a much smaller required k_{\max} in many-body simulations. When the averaging process in the partial averaging method is continued through *all* of the Fourier variables, the Feynman-Hibbs effective potential [2] is obtained.

We just summarize the steps of the derivation here and refer the reader to Ref. [31] where the procedure is outlined in an exercise. We first make approximation (1.25) for the inner average over the a_k variables in Eq. (1.22). We are then interested in the average of the difference between the interaction energy of the solute along the path and that evaluated at the centroid. But we note that no point along the path is special, and we choose the point x for our sampling point; \bar{x} remains fixed. Since the variable x is generated by a linear combination of the a_k variables, the multidimensional Gaussian can be collapsed into a single Gaussian integral after some algebra [48]:

$$\Delta\Delta U_{\alpha}^{\text{eff}}(\bar{x}) = \frac{\int dy [\Delta U_{\alpha}(\bar{x} - y) - \Delta U_{\alpha}(\bar{x})] e^{-\frac{6my^2}{\beta\hbar^2}}}{\int dy e^{-\frac{6my^2}{\beta\hbar^2}}}. \quad (1.26)$$

Here $\Delta\Delta U_{\alpha}^{\text{eff}}(\bar{x})$ is an effective potential representing the quantum deviations from the classical interaction potential. This effective potential is variational since the only approximation made so far is from the inequality (1.25).

Now if we assume that the deviations are small, and expand $\Delta U_{\alpha}(\bar{x} - y)$ about the point \bar{x} to second order, we get

$$\boxed{\Delta\Delta U_\alpha^{\text{eff}}(\bar{x}) \approx \frac{\beta\hbar^2}{24m} \Delta U_\alpha''(\bar{x})}, \quad (1.27)$$

where $\Delta U_\alpha''(\bar{x})$ is the second derivative of the potential evaluated at \bar{x} . We will call this the Quadratic Feynman-Hibbs (QFH) correction. Kleinert [43] shows that this quadratic expansion is also variational; all approximations derived beyond this one may remove this property. For a pairwise interaction, the QFH correction reads:

$$\Delta\Delta U_\alpha^{\text{eff}}(\bar{x}) \approx \frac{\beta\hbar^2}{24\mu} \left[\Delta U_\alpha''(r) + 2\frac{\Delta U_\alpha'(r)}{r} \right], \quad (1.28)$$

where μ is the reduced mass, and the derivatives $\Delta U''$ and $\Delta U'$ are taken with respect to the scalar distance between the atoms.

The QFH potential approximately captures two key quantum effects. When an atom is near a potential minimum, the curvature is positive and thus so is the QFH correction; this models the zero-point effect. On the other hand, near potential maxima the curvature is negative, and the QFH potential models tunneling.

The Feynman-Hibbs and QFH potentials have been used extensively in simulations examining quantum effects in atomic and molecular fluids [15, 27, 12]. We note here that the centroid molecular dynamics method [52, 53] is related and is intermediate between a full path integral simulation and the Feynman-Hibbs approximation; the averaged forces during the classical propagation are determined using a path integral simulation. It has been shown that the QFH potential and the centroid approach yield similar results in water simulations [27].

We can view obtaining the QFH correction to the excess chemical potential in two ways. If we simply plug Eq. (1.27) back into Eq. (1.22), this suggests that we first compute the classical excess chemical potential and then insert the classical solute into the system and evaluate

$$\boxed{-\ln\langle e^{-\frac{\beta^2\hbar^2}{24m}\Delta U_\alpha''(\bar{x})} \rangle_{\text{cl}}} \quad (1.29)$$

for the quantum correction. Alternatively, we can recombine the classical and quantum correction terms in Eq. (1.22) and calculate the excess chemical potential as

$$\beta\mu_\alpha^{\text{ex,QFH}} = -\ln\langle e^{-\beta[\Delta U_\alpha(\bar{x}) + \frac{\beta\hbar^2}{24m}\Delta U_\alpha''(\bar{x})]} \rangle_0. \quad (1.30)$$

If we are interested in the excess chemical potential change for mutating mass m_A into mass m_B , we obtain

$$\begin{aligned} \beta\Delta\mu_\alpha^{\text{ex,QFH}}(m_A \rightarrow m_B) &= -\ln \frac{\langle e^{-\beta[\Delta U_\alpha(\bar{x}) + \frac{\beta\hbar^2}{24m_B}\Delta U_\alpha''(\bar{x})]} \rangle_0}{\langle e^{-\beta[\Delta U_\alpha(\bar{x}) + \frac{\beta\hbar^2}{24m_A}\Delta U_\alpha''(\bar{x})]} \rangle_0} \\ &= -\ln\langle e^{-\frac{\beta^2\hbar^2}{24}\Delta(\frac{1}{m})\Delta U_\alpha''(\bar{x})} \rangle_{m_A}, \end{aligned} \quad (1.31)$$

where $\Delta(1/m) = 1/m_B - 1/m_A$ and again we have used Eq. (1.5). The calculation is performed with the mass m_A particle included, interacting with the rest of the system with the QFH potential.

Feynman and Kleinert have derived a method which is a significant improvement over the Feynman-Hibbs variational approach. A detailed discussion of this method is given in Ref. [43]. The method focuses on a local harmonic oscillator reference system rather than performing the Gaussian integrals directly as done above. The derived effective potential goes to the classical potential at high temperatures, but in addition gives a remarkably good estimate of the ground state energy at low temperatures. The approximated free energy is an upper bound, just like in the Feynman-Hibbs method, but a better approximation is obtained at lower temperatures. It does involve increased complexity in obtaining an optimal local harmonic frequency. Moreover, the applications considered here are mainly in the higher-temperature regime discussed in Ref. [43].

Another issue to mention concerns the sampling of the solvent degrees of freedom. The cl subscript on the outside average of the last term of Eq. (1.22) refers to treating the *solute* classically. If the solvent is expected to display minor quantum effects, then it too can be modeled with a QFH potential; the solute should be treated classically in the cl-labelled averaging though. If the interaction potential happens to be a pairwise potential, then a very simple form for the QFH potential results [15, 27, 12], as shown in Eq. (1.28).

1.8 A Worked Example

We have covered a lot of ground starting from an exact quantum PDT and deriving a physically based Feynman-Hibbs effective potential designed to approximately include quantum effects during a classical calculation. The path integral methods used to derive the Feynman-Hibbs potential are involved, but the result Eq. (1.26) is simple: Take a Gaussian smear of the potential centered at the classical point \bar{x} . Here we stop and consider an example, the harmonic oscillator, which illustrates some of the results discussed above. The harmonic oscillator partition function, and thus the Helmholtz free energy, is easy to obtain analytically. The exact free energy is

$$A_{\text{QM}} = \frac{1}{\beta} \ln \left[\sinh \left(\frac{\hbar\omega\beta}{2} \right) \right], \quad (1.32)$$

where ω is the harmonic frequency. The high temperature or classical limit of this expression is

$$A_{\text{CM}} = \frac{1}{\beta} \ln(\hbar\omega\beta). \quad (1.33)$$

Using path integral methods, Feynman [2] showed that the Feynman-Hibbs form for the harmonic oscillator free energy is

$$A_{\text{FH}} = \frac{1}{\beta} \left[\ln(\hbar\omega\beta) + \frac{\hbar^2\beta^2\omega^2}{24} \right]. \quad (1.34)$$

This approximation can also be easily obtained from the expression (1.29). Based on our discussion above, we expect $A_{\text{CM}} < A_{\text{QM}} < A_{\text{FH}}$. Figure 1.1 illustrates these bounds. The Feynman-Hibbs free energy provides a very good representation at moderate temperatures at which some excited states are populated. See Kleinert's book [43] for applications to anharmonic systems.

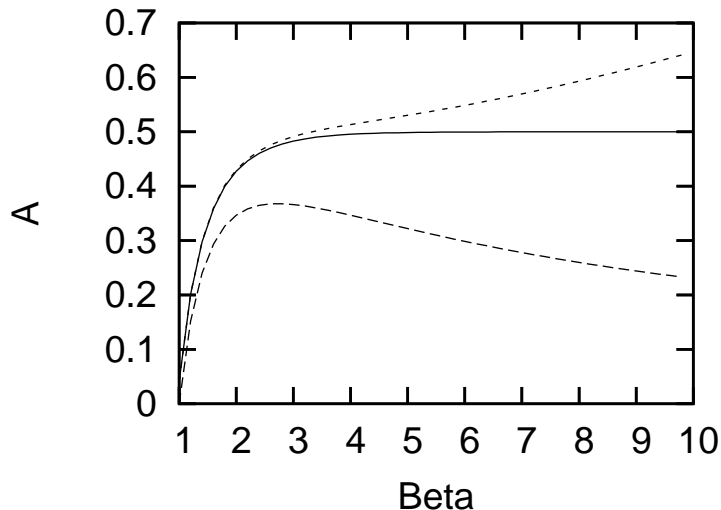


Fig. 1.1. The Helmholtz free energy as a function of β for the three free energy models of the harmonic oscillator. Here we have set $\hbar = \omega = 1$. The exact result is the solid line, the Feynman-Hibbs free energy is the upper dashed line, and the classical free energy is the lower dashed line. The classical and Feynman-Hibbs potentials bound the exact free energy, and the Feynman-Hibbs free energy becomes inaccurate as the quantum system drops into the ground state at low temperature.

We will finish the example with a couple of points which will prove useful later in the chapter. If we insert the harmonic oscillator potential into the temperature correction formula (1.2), we get

$$\frac{1}{12}(\beta\hbar\omega)^2 T \quad (1.35)$$

for the correction. At room temperature, $\beta^{-1} \approx 208 \text{ cm}^{-1}$ in typical units for vibrational frequencies, so the correction is $25(\tilde{\nu}/208)^2$. If we assume a frequency of 294 cm^{-1} , we get a temperature correction of 50 K. By examining the density of states for liquid water [54], the choice of a few hundred cm^{-1}

as a characteristic frequency is not unreasonable. The high density of states in that frequency range is due to the hindered rotations of the water molecules in the liquid. As we will see below, the quantum effects on the structural properties of liquid water are roughly equivalent to a 50 K temperature rise in the classical liquid.

Second, there has been a discussion of whether it is better to treat the water molecule as rigid or flexible during simulations of the fluid [38]. One argument has been that, since the molecules are largely in their ground vibrational states at room temperature, it might be better to treat them as rigid. But this assumption seems somewhat questionable when the rms proton fluctuations ($\sqrt{\langle x^2 \rangle}$) are calculated in the classical and quantum (ground state) limits. Let's assume a harmonic oscillator with a vibrational frequency of roughly 1500 cm^{-1} , a mass of 2 proton masses, and a temperature of 300 K. These parameters lead to classical and quantum predictions of the rms fluctuations of 0.04 and 0.075 Å, respectively. So the notion that the molecule is effectively more rigid in the quantum system may not be physically correct.

1.9 Wigner-Kirkwood Approximations

Wigner-Kirkwood related expansions follow by taking the approximations further. We assume Eq. (1.30) as a starting point and linearize the exponential of the correction term for the potential:

$$-\ln\langle e^{-\beta[\Delta U_\alpha(\bar{x}) + \frac{\beta\hbar^2}{24m}\Delta U_\alpha''(\bar{x})]} \rangle_0 \approx -\ln \frac{\int dx^N e^{-\beta U_N} e^{-\beta\Delta U_\alpha(\bar{x})} \left(1 - \frac{\beta^2\hbar^2}{24m}\Delta U_\alpha''(\bar{x})\right)}{\int dx^N e^{-\beta U_N} e^{-\beta\Delta U_\alpha(\bar{x})}} - \ln \frac{\int dx^N e^{-\beta U_N} e^{-\beta\Delta U_\alpha(\bar{x})}}{\int dx^N e^{-\beta U_N}}, \quad (1.36)$$

assuming the total potential for the solvent U_N is a classical potential for now.

The second term on the right of Eq. (1.36) is just the classical excess chemical potential. The first term is

$$-\ln \left[1 - \frac{\beta^2\hbar^2}{24m} \langle \Delta U_\alpha''(\bar{x}) \rangle_{\text{cl}} \right], \quad (1.37)$$

which also can be obtained by expanding the exponential in (1.29). An effective potential closely related to (1.37) was derived by Stratt [42] and has been examined in molecular simulations [12]. Expanding the logarithm, we get:

$$\beta\mu_\alpha^{\text{ex,WK}} \approx \beta\mu_\alpha^{\text{ex,cl}} + \frac{\beta^2\hbar^2}{24m} \langle \Delta U_\alpha''(\bar{x}) \rangle_{\text{cl}}. \quad (1.38)$$

Now consider the classical average of the second derivative appearing in Eq. (1.38). This average can be integrated by parts if we assume a very large system where the boundary effects are negligible [41]:

$$\beta\mu_{\alpha}^{\text{ex,WK}} \approx \beta\mu_{\alpha}^{\text{ex,cl}} + \frac{\beta^3 \hbar^2}{24m} \langle (\Delta U'_{\alpha}(\bar{x}))^2 \rangle_{\text{cl}}. \quad (1.39)$$

This is of the form of the correction to the free energy in Eq. (1.1). Extensions for rigid molecules are given in Ref. [55].

By performing the integration by parts on only a portion of the correction, we can also say

$$\beta\mu_{\alpha}^{\text{ex,WK}} \approx \beta\mu_{\alpha}^{\text{ex,cl}} - \frac{\beta^3 \hbar^2}{24m} \langle (\Delta U'_{\alpha}(\bar{x}))^2 \rangle_{\text{cl}} + \frac{\beta^2 \hbar^2}{12m} \langle \Delta U''_{\alpha}(\bar{x}) \rangle_{\text{cl}}. \quad (1.40)$$

If we now re-express Eq. (1.40) as the expansion of a logarithm, and then re-exponentiate the terms inside the classical average, we obtain Eq. (1.3) as an effective potential.

At this point it might be helpful to summarize what has been done so far in terms of effective potentials. To obtain the QFH correction, we started with an exact path integral expression and obtained the effective potential by making a first-order cumulant expansion of the Boltzmann factor and analytically performing all of the Gaussian kinetic energy integrals. Once the first-order cumulant approximation is made, the rest of the derivation is exact up to Eq. (1.26). A second-order expansion of the potential then leads to the QFH approximation.

Once the QFH formula for the excess chemical potential is linearized in Eq. (1.37), the logarithmic expression can be expanded to first order and all or part of the classical-average term can be integrated by parts to yield the Wigner-Kirkwood correction to the free energy. Then if Eq. (1.40) is reorganized, computation of the chemical potential can be viewed as a classical average with a modified interaction potential of the same form as Eq. (1.3).

How do the two effective potentials compare? In Ref. [12], the effective potentials corresponding to Eqs. (1.27), (1.37), and (1.40) are plotted for neon at its triple-point temperature. All three effective potentials mimic zero-point motion by raising the potential near the minimum relative to the classical Lennard-Jones form. The potentials differ widely at small separations, however. The QFH approximation is more repulsive than the classical potential at small r values, while the logarithmic form of the Wigner-Kirkwood effective potential Eq. (1.37) is less repulsive than the classical potential. Also, this logarithmic form of the Wigner-Kirkwood potential matches up quite well at small r with path integral calculations for the atomic pair [13]. The effective potential Eq. (1.3) derived from Eq. (1.40) exhibits an unphysical negative divergence at small r due to the negative sign in front of the square of the gradient of the interaction potential.

At first glance, it would appear that the QFH approximation is a better one since it is only a few steps removed from the exact path integral results, and the Wigner-Kirkwood formulas are obtained only after several subsequent approximations. However, the Wigner-Kirkwood pair potential is closer to a

path-integral-derived effective potential at small distances. There doesn't appear to be a conclusive comparison of the two effective potentials for all of the thermodynamic and structural properties of fluids, although there has been significant work in this direction [11, 15]. Sese concludes that the QFH approximation performs better in computing thermodynamic properties compared with path integral results. He does note that QFH-derived pressures deviate from the exact results at low temperatures and/or high densities. This is probably due to the enhanced repulsive character of the potential. Also, he showed that a Gaussian deconvolution of the center-of-mass QFH radial distribution function leads to much better agreement with experiment [15]. Previously he had found that Wigner-Kirkwood models gave better agreement with experimental structural data [17]. The reader is referred to more extensive discussion of the relative merits of the effective potentials in these original papers.

1.10 The PDT and Thermodynamic Integration for Exact Quantum Free Energy Changes

Say you have performed a classical calculation to determine the excess chemical potential from the first two terms on the right side of Eq. (1.22) followed by another classical calculation to obtain an estimate of the quantum correction from the expression (1.29), and the estimated correction is large. This suggests that a full quantum treatment is necessary. In this section we derive the appropriate formulas for changes in the excess chemical potential due to mutating masses. If the original mass is very large, which corresponds to the classical limit, the derived expressions yield the quantum correction.

Consider a problem, in which we are interested in the mass-dependent partitioning of a solute between an ideal gas phase and a condensed phase. The ratio of the densities in the two phases or the partition coefficient for species α is then

$$K = e^{-\beta\mu_\alpha^{\text{ex}}}, \quad (1.41)$$

where μ_α^{ex} is the excess chemical potential in the condensed phase. Thus to calculate the ratio of the partition coefficients for two isotopes, we need only consider the difference in the excess chemical potentials, and that will be our focus here.

Let's first examine changes in the quantum correction of Eq. (1.22) due to a change in mass. For that change we obtain

$$-\ln \frac{\left\langle \left\langle e^{-\beta \int_0^1 [\Delta U_\alpha[x(\tau)] - \Delta U_\alpha(\bar{x})] d\tau} \right\rangle_{a_k, \text{B}} \right\rangle_{\text{cl}}}{\left\langle \left\langle e^{-\beta \int_0^1 [\Delta U_\alpha[x(\tau)] - \Delta U_\alpha(\bar{x})] d\tau} \right\rangle_{a_k, \text{A}} \right\rangle_{\text{cl}}}. \quad (1.42)$$

We will use Eq. (1.5) yet again, but we should be careful to note that the normalization integrals for the numerator and denominator are slightly different.

Taking care of those terms, we get

$$\beta\Delta\mu_\alpha^{\text{ex}}(m_A \rightarrow m_B) = -\frac{3k_{\text{max}}}{2} \ln \frac{m_B}{m_A} - \ln \left\langle e^{-\frac{\pi^2 \Delta m}{4\beta\hbar^2} \sum_k a_k^2 k^2} \right\rangle_{m_A}, \quad (1.43)$$

where $\Delta m = m_B - m_A$, and 3 in the first term on the right side comes from assuming the particle moves in three dimensions. In that case, the sum in the exponent of the second term should be over all the solute Fourier variables for the three dimensions. In the averaging of the second term it is assumed that the mass m_A particle is included in the system. If the mass change is not too large, this expression should suffice. But if there is a significant mass change and the quantum effects are large, the statistical averaging will be noisy. In fact, this is a somewhat disturbing limit since as we let the initial mass m_A approach infinity, we get the difference of two infinite terms, which should in the end yield a well-defined and finite result. We will see later that calculating the excess chemical potential in this limit is not so bad as it first appears. For practical purposes, we can break up the mutation process into a sequence of smaller mass changes, using Eq. (1.43) for each step. See Chapter 2 in this book for a discussion of perturbation theory.

Alternatively, the mass change can be enacted by thermodynamic integration. It is shown in Ref. [31] that thermodynamic integration possesses excellent scaling properties so long as the free energy changes smoothly with the scaling parameter. This provides a good reason for its workhorse status in free energy calculations. We will assume that the mass m_B is smaller than the mass m_A with an eye towards the transition from classical to quantum limits. Take the second term on the right side of Eq. (1.43) and replace Δm with $(1-\lambda)m_B$. We will consider the transition from $\lambda = 1$ to $\lambda = \lambda_f$, where $m_A = \lambda_f m_B$. This creates the λ -dependent function $F(\lambda)$:

$$F(\lambda) = -\ln \left\langle e^{-\frac{\pi^2 (1-\lambda)m_B}{4\beta\hbar^2} \sum_k a_k^2 k^2} \right\rangle_{m_A}. \quad (1.44)$$

Then we can integrate the derivative of this function to get our desired result:

$$F(\lambda_f) - F(1) = \int_1^{\lambda_f} \frac{\partial F}{\partial \lambda} d\lambda, \quad (1.45)$$

since $F(\lambda_f)$ is what we seek and $F(1) = 0$. Once we calculate the derivative and assemble the averages, we get for the quantum correction

$$\beta\Delta\mu_\alpha^{\text{ex}}(m_A \rightarrow m_B) = -\frac{3k_{\text{max}}}{2} \ln \frac{m_B}{m_A} - \frac{\pi^2 m_B}{4\beta\hbar^2} \int_1^{\lambda_f} \left\langle \sum_k a_k^2 k^2 \right\rangle_\lambda d\lambda. \quad (1.46)$$

The λ -dependent averaging inside the integral involves a path integral simulation with the particle of interest involved but with a mass of $m_A + (1-\lambda)m_B$. This formula was used to estimate isotope effects on solubilities of hydrogen

and deuterium in model anharmonic solids in Ref. [46]. A similar expression was derived for Cartesian path integrals by Runge and Chester [23]. We are considering the transition from a large mass to a small mass, so $\lambda_f > 1$ and the second term is thus always negative due to the minus sign in front. But the net result for the quantum correction is positive [51], so the first term must exceed the second in magnitude. That first term is always positive for $m_A \gg m_B$. Eq. (1.46) appears similar to the T method of kinetic energy estimation [20]. It has been noted that the standard deviation of the kinetic energy in the T method increases as the square root of k_{\max} [20]. The growth of the standard deviation is not surprising due to the k^2 factor. Predescu and Doll [56], building on fundamental ideas from Brownian motion theory, have proposed a reweighting scheme for the Fourier method which yields better-convergent estimators, and Mielke and Truhlar [57] have compared various Fourier-based estimators in free energy calculations.

Physically, as we go to larger masses during the λ integration, the widths of the Gaussians in the kinetic energy piece of the sampling function become very narrow. This means that the distributions of the a_k 's are essentially Gaussian due to no influence from the potential; on the scale of the very small particle fluctuations, the potential does not vary. If we assume that the kinetic and potential pieces have decoupled in this way, then we can perform the Gaussian integrals in the $\langle \dots \rangle_\lambda$ averages analytically, and indeed we get exactly the opposite of the first term in Eq. (1.46). This suggests that we perform the λ integration as given in Eq. (1.46), successively increasing m_A until the process converges to a stable value; we have then reached the classical limit.

We can view the classical \rightarrow quantum transition another way, namely through the potential rather than the kinetic energy. If we substitute $(1 - \lambda)\Delta U_\alpha(\bar{x}) + \lambda\Delta U_\alpha[x(\tau)]$ for $\Delta U_\alpha[x(\tau)]$ in the quantum correction term of Eq. (1.22), and then follow through with a thermodynamic integration procedure, we obtain

$$\beta[\mu_\alpha^{\text{ex,QM}} - \mu_\alpha^{\text{ex,CM}}] = \beta \int_0^1 \left\langle \int_0^1 [\Delta U_\alpha[x(\tau)] - \Delta U_\alpha(\bar{x})] d\tau \right\rangle_\lambda d\lambda, \quad (1.47)$$

where now the path integral λ -dependent averaging uses the mixed potential given above. The $\lambda = 0$ limit is the classical limit, and $\lambda = 1$ generates the full quantum correction. This method presumably does not suffer from the k_{\max} -dependent statistical sampling issue in Eq. (1.46), but we are not aware of a direct comparison of the two views of the classical \rightarrow quantum transition. The approach of Eq. (1.47) was used by Morales and Singer [14] in calculations of free energies for liquid neon.

1.11 Assessment and Applications

As we have seen, the Potential Distribution Theorem gives a compact means to derive quantum corrections to the classical chemical potential for an atomic or molecular solute. By making a variational approximation, the Feynman-Hibbs effective potential emerges directly from the exact path integral expression. If we expand the potential about the centroid to second order, the QFH approximation results, and the Wigner-Kirkwood approximations are obtained from further approximations. The classical excess chemical potential and the QFH quantum approximation give lower and upper bounds, respectively, to the exact quantum result. Thus, using purely classical simulation, we can begin to get a handle on the importance of quantum effects for free energies of a fluid. We will see below that, if the estimated quantum correction to the chemical potential is roughly 15% of the classical value or larger, then we should probably consider using a full path integral treatment. It is recommended to use the QFH potential (Eq. (1.27)) for the estimate of the quantum correction of thermodynamic properties since it is easy to incorporate during a classical simulation and is closest to the exact quantum result as we proceed down the ‘approximation chain’ – see Section (1.9). For most of the problems of interest to molecular modelers, the quantum effects are expected to be relatively weak, so these approximate methods are likely to give good estimates.

In this section, we will discuss some examples from the literature which have used the approximation methods derived in this chapter. In several cases, the approximations have been compared with more accurate path integral simulations to assess their validity. This is not meant as a full review; rather, several case studies have been chosen to illustrate the tools we have developed. We will first look at simpler examples and then discuss water models and applications in enzyme kinetics.

1.11.1 Foundational Examples

As noted above, Wang *et al.* [9] utilized the exact form of the quantum PDT in studies of liquid para-hydrogen and neon. For para-hydrogen, they found large differences between the free energies with classical or quantum models at low temperatures: At 30K, the quantum result is roughly -250 kJ/kg, while the classical prediction is -750 kJ/kg. The quantum and classical results do not converge until roughly 120 K. The deviations for liquid neon are much less, on the order of 15 kJ/kg at 30 K, and the classical and quantum calculations converge around 50 K. The quantum results for both cases agree well with experimental data. These simulations confirm that hydrogen is a highly quantum liquid, while neon exhibits small but non-negligible quantum effects at low temperatures. Ortiz and Lopez [16] calculated adsorption isotherms for a neon monolayer using the quantum PDT, and observed an appreciable shift of the isotherms due to quantum effects at low temperatures. Morales and Singer [14] computed quantum corrections to the classical Helmholtz free

energy for liquid neon at the triple point and observed a 5% change with inclusion of quantum effects. The Gibbs free energy, on the other hand, changes by 15% due to large changes in the ratio of the pressure to the density. They also tested a Wigner-Kirkwood model and found a 10% overestimation of the quantum correction obtained from an expansion to 2nd-order in \hbar . By adding a 4th-order term, the Wigner-Kirkwood error is reduced to about 5%. The free energy computed with path integral simulations agrees with experiment to within 3% of the measured value.

Sese presented a more thorough examination of approximate quantum models for neon [15], namely the Feynman-Hibbs and QFH models. Free energies were calculated using the PDT. The Gibbs free energy from the models is always higher than the value computed using path integral methods, and the classical free energy is below the path integral result. This is expected considering the variational bounds discussed above. Four state points were examined. For state point 2, with a reduced temperature of 0.9517 and reduced density of 0.7246, the calculated Gibbs free energy differs from path integral results by 2% and 3% for the Feynman-Hibbs and QFH models, respectively. The classical prediction differs from the path integral value by 8%, and the path integral result is 1% in error relative to experiment. The agreement between the Feynman-Hibbs models and path integral simulations is not as good at a lower temperature and higher density state point where the classical and quantum Gibbs free energies differ by 14%. Sese defined a dimensionless parameter $\Lambda^* = (\hbar^2/2\pi mk_B T \sigma^2)^{1/2}$ which gives the ratio of the quantum spread to the Lennard-Jones size parameter σ . When the reduced density is less than 0.89, the reduced temperature greater than 0.60, and $\Lambda^* \leq 0.28$, accurate thermodynamics can be obtained with the Feynman-Hibbs models.

Tchouar *et al.* [12] also utilized the QFH potential in simulations of neon, methane, and gas helium at low temperatures. They did not compute free energies, but obtained excellent agreement between the QFH and path integral calculations for the average total energies of the systems. They found similar conditions of validity to those given by Sese [15]. They also found much better agreement with experiment for diffusion constants and shear viscosity coefficients when the classical potentials were substituted with the QFH form, thus indicating these effective potentials may also be useful for dynamical quantities.

- *The Feynman-Hibbs and QFH models perform quite well in free energy calculations so long as the quantum corrections are modest. The conditions for validity of the approximations are given above.*

1.11.2 Forcefield Models of Water

Moving on to quantum effects in water, we'll first examine forcefield models of water, and then discuss recent *ab initio* simulation results. Early works

utilizing path integral methods to study quantum effects in water include those by Kuharski and Rossky [58] and Wallqvist and Berne [59]. Kuharski and Rossky used a rigid (ST2) model of water, while Wallqvist and Berne examined a flexible model. Both observed a destructuring of the fluid with the inclusion of quantum effects. Kuharski and Rossky estimated the quantum correction to the free energy with a Wigner-Kirkwood model, obtaining a value of 0.68 kcal/mol for H₂O. The major contributor to this correction is the librational component, not translations which comprise less than 10% of the total correction. The excess chemical potential of water is -6.1 kcal/mol [34], so the estimated quantum correction is roughly 10% of the total. By differentiating the free energy with respect to temperature, they also estimated the quantum correction to the averaged interaction energy as 1.24 kcal/mol. The experimental total binding energy is -9.92 kcal/mol [54]. The larger magnitude for the energetic portion of the quantum correction implies a positive entropic contribution. Using path integral methods, their estimate of the energetic change was 0.82 kcal/mol. Reduced quantum corrections were observed for D₂O.

In more recent path integral studies, Stern and Berne [54] examined a forcefield for flexible water obtained from *ab initio* calculations. Their classical simulation produced a total binding energy of -11.34 kcal/mol, while their path integral result was -9.8 kcal/mol, very close to the experimental value. The estimate of the quantum correction to the binding energy of 1.5 kcal/mol is slightly larger than previous estimates. A simple harmonic model predicts a correction of 1.7 kcal/mol. In their flexible model, convergence of the energy of an isolated monomer is not obtained until more than 30 beads are included in the Cartesian path integral simulations.

Mahoney and Jorgensen [32] studied quantum, flexibility, and polarizability effects on water. They also developed a modified TIP5P(PIMC) rigid water potential, where the parametrization was based on path integral rather than classical simulations. Serious attention was paid to reproducing the temperature of maximum density. A Cartesian discretization with 5 beads was found sufficient to obtain converged results for rigid water models. For the TIP5P(PIMC) model, the authors observed an average intermolecular energy of -9.94 kcal/mol, close to the -9.92 kcal/mol experimental value. Also, the predicted heat of vaporization is 10.53 kcal/mol *vs.* the experimental value of 10.51 kcal/mol. The quantum correction to the interaction energy for the TIP5P model is 1.6 kcal/mol, consistent with the results of Stern and Berne [54]. Mahoney and Jorgensen argue that real water is better approximated by rigid water models than by classical flexible models. We note here that there has also been significant recent effort devoted to developing classical forcefield models which accurately reproduce spectroscopic data for water clusters [60].

These path integral simulations serve as benchmarks for approximate models. Guillot and Guissani [27] employed the QFH approximation in extensive simulations of structure and dynamics in water and D₂O. A modified flexible forcefield was used. The QFH model predicts a heat of vaporization of 9.42

kcal/mol (corrected for zero-point differences) for water compared with path integral predictions of 9.79 kcal/mol (ST2 model) and 10.84 kcal/mol (SPC/E model), and an experimental value of 9.66 kcal/mol. The quantum correction to the heat of vaporization predicted with the QFH model is 1.23 kcal/mol *vs.* the path integral predictions of 1.18 kcal/mol and 1.27 kcal/mol. Therefore, it appears the QFH model gives an excellent estimate of this thermodynamic quantity. The quantum contribution to the heat of vaporization is roughly 12% for water, a significant value. Guillot and Guissani noted an interesting discrepancy between the simulations and experimental results: The partial molar volume of D₂O is *greater* than that for water, and the QFH model does not reproduce this property. As for atomic fluids [15], for a given volume the pressure increases with inclusion of quantum effects, and a higher pressure is thus observed for water compared with D₂O in the QFH simulation. This may be related to the enhanced repulsive character of the QFH effective potential discussed above in Section (1.9). The temperature of maximum density shift is reasonably well-reproduced with the QFH model. The authors also examined extensively the structural and dynamical properties of water. Consistent with many other simulations, the radial distribution functions soften with the inclusion of quantum effects, and diffusion is enhanced. The ratio of diffusion constants for water and D₂O increases markedly as the temperature is decreased; this quantity is also accurately reproduced by the QFH model. This study suggests that the QFH approximate model can accurately predict thermodynamic properties of water. The authors also compared their results with those from a more costly centroid molecular dynamics simulation of water [52], and found excellent agreement between the two methods.

- *Inclusion of quantum effects leads to a destructuring of water.*
- *The quantum contribution to the excess chemical potential is roughly 10% of the total.*
- *The librational component is the major contributor to the quantum correction.*
- *The interaction-energy contribution to the quantum correction is larger in magnitude than the free energy contribution, suggesting the entropic part is positive.*
- *Modified forcefield models based on path integral simulations yield excellent agreement with experiment for thermodynamic properties.*
- *Flexible forcefield models require 30 or more beads in Cartesian path integral descriptions to obtain converged intramolecular energies. Rigid water models require only about 5 beads due to the weaker intermolecular quantum effects.*
- *Rigid water models appear to better represent real water than flexible classical models.*
- *The QFH effective potential gives good agreement with path integral results for the thermodynamic properties of water.*

- *Diffusion constants are enhanced with the approximate inclusion of quantum effects. Changes in the ratio of diffusion constants for water and D₂O with decreasing temperature are accurately reproduced with the QFH model. This ratio computed with the QFH model agrees well with the centroid molecular dynamics result at room temperature. Fully quantum path integral dynamical simulations of diffusion in liquid water are not presently possible.*

1.11.3 *Ab Initio* Water

Finally, we mention recent *ab initio* simulations of liquid water. This promising area for fundamental studies of water thermodynamics, structure, reactivity, and dynamics is in active development. Calculations using different DFT functionals and different computational methods have resulted in quite different properties for water [34], and we make no attempt to assess these differences here. Generally, if the nuclei are propagated with classical mechanics, an overstructured liquid is observed, and the diffusion constant is much smaller than the experimental value. These differences could be due to the neglect of quantum effects on the proton motions, deficiencies in the DFT functionals, or lack of convergence in the calculations. Proton quantum effects during an *ab initio* simulation have been included in the recent study of Chen *et al.* [33], but there is some question as to convergence of the simulation with the path integral discretization number P [37]. Schwegler *et al.* [37] found that the experimental radial distribution functions could be accurately reproduced by increasing the temperature in classical simulations by roughly 50 K for simulations using a rigid water structure and 100 K for a flexible water model.⁷ They suggested that this temperature increase is consistent with path integral results using the TIP5P(PIMC) model discussed above, and thus quantum effects on proton motion are significant. The correspondence of quantum effects with a 50 K temperature rise seems quite large, but if one estimates the change in excess chemical potential from $\Delta\mu^{ex} = -s_i\Delta T$, where s_i is the partial molar entropy of classical water, a 50 K temperature rise yields a chemical potential change of roughly 1 kcal/mol, consistent with previous estimates from path integral studies [58]. And, as discussed in Section (1.8), a reasonable estimate of the temperature correction for liquid water using Eq. (1.2) is also 50 K. This finding is further supported by recent centroid molecular dynamics simulations [62].

Allesch *et al.* [38] also carried out *ab initio* simulations of rigid water molecules and observed a decrease in water structure relative to a flexible water simulation. It was argued that, since the water is predominantly in the ground vibrational state at room temperature, it is not surprising rigid models seem to more accurately mimic water properties. Calculations of the

⁷A recent *ab initio* study [61] has also shown that the melting point with neglect of quantum effects is elevated to nearly 400 K.

rms fluctuations in classical or quantum ground state harmonic models call this argument into question, however – see Section (1.8). It is also possible that the underlying DFT functionals contain deficiencies which are difficult to disentangle from other contributions to the structure and thermodynamics [34, 35, 60]. Two of the most commonly used DFT functionals (PBE and BLYP) lead to very similar and over-structured radial distribution functions [63], while a modification of the PBE functional (rPBE) produces a less-structured fluid [34, 35].

The only estimate of the free energy of water determined from *ab initio* simulation is Ref. [34]. This ground-breaking work utilized data from *ab initio* simulation in conjunction with quasi-chemical theory to estimate the excess chemical potential of water in water. The quasi-chemical treatment partitions the problem into inner-sphere chemical effects and outer-sphere packing, electrostatic, and van der Waals effects [31]. Information theory, using occupancy statistics, yields estimates of the chemical and packing contributions. The theory can also be checked variationally by altering the inner-sphere radius. One key conclusion from these calculations is that the inner-sphere chemical effects nearly balance the outer-sphere packing effects. The estimates of the independent contributions to the chemical potential lead to helpful insights into the various contributions, and the estimated final value of -5.1 kcal/mol is quite close to the experimental value of -6.1 kcal/mol. When a molecular-level simulation result is substituted for a simple dielectric model for the outer-sphere electrostatics, the prediction changes to -7.5 kcal/mol. With a quantum correction of roughly 0.7 kcal/mol, the final prediction would be about -6.8 kcal/mol, within $k_B T$ of the experimental result. The DFT functional (rPBE) used in this study is perhaps not of such a high quality to expect such remarkable agreement, but it is noteworthy that such a close estimate is possible. Quantum effects can also be expected for the proton in water, and steps towards modeling those effects are discussed in Refs. [64] and [31]. There is a lot of interest in extending ideas developed in fundamental studies of the proton in water to examine energetics and pathways for proton motion through membrane proteins [65, 66, 67, 68, 69].

- *Ab initio simulations of water using classical propagation generally lead to an overstructured liquid compared with experiment.*
- *Deviations from experiment could be due to the neglect of quantum effects, overestimation of the flexibility of water in the liquid, deficiencies in the DFT functionals, or lack of convergence in the computational methods.*
- *Treating water as a rigid molecule in ab initio simulations leads to a de-structuring of the fluid relative to classical flexible water.*
- *The radial distribution functions in ab initio simulations agree with experiment if the temperature is raised by roughly 50 K, consistent with results from the TIP5P(PIMC) forcefield model. This implies that quantum effects are non-negligible.*

- *A quasi-chemical theory, using ab initio simulation (rPBE functional) to generate data for the computation of the various contributions to the free energy, yields an estimate for the excess chemical potential of water very close to the experimental value.*

1.11.4 Enzyme Kinetics

Most of the discussion in this chapter has concerned equilibrium quantities, free energies in particular. How might the methods discussed here apply to kinetic phenomena? An area with significant current interest is the utilization of quantum methods to study the kinetics of enzyme reactions [21, 22]. The underlying theory typically employed is transition state theory (TST). In TST it is assumed that there is a local equilibrium along the path linking the reactants and the transition state. The central quantities in TST are the free energy of activation and the transmission coefficient. The methods discussed in this chapter are directly applicable to computing the free energies of activation in complex systems. The PDT allows a local definition of the free energy which can be followed along the progression of the reaction. Thus, in principle the free energy profile can be calculated from reactants to the transition state, or rather the ensemble of transition states.

Extensive theoretical work has been directed at understanding nuclear quantum effects on enzyme kinetics. These quantum effects enter in two ways. First, there can be a change in the system zero point energy between the reactants and the transition state. Second, there can be tunnelling effects which show up in the transmission coefficient and in the activation free energy. The Feynman-Hibbs models at least approximately account for both of these effects: The effective potential is raised in regions where the force constant is positive (potential minima) and lowered near transition states (potential maxima). If the quantum effects are large, then path integral methods can be implemented to compute more accurate free energies along the reaction coordinate.

As an example, consider an early calculation of isotope effects on enzyme kinetics by Hwang and Warshel [21]. This study examines isotope effects on the catalytic reaction of carbonic anhydrase. The expected rate-limiting step is a proton transfer reaction from a zinc-bound water molecule to a neighboring water. The transition-state-theory expression for the rate constant k is

$$k = F \frac{k_{\text{B}}T}{h} \exp(-\beta\Delta g^{\ddagger}), \quad (1.48)$$

where F is the transmission factor, and Δg^{\ddagger} is the free energy of activation. As discussed above, the free energy of activation is calculated as a difference between the reactant and transition states, and can be viewed as the difference of local excess chemical potentials with the particle centroid situated at those two locations. The major contributor to the quantum effects in proton transfer comes through the Boltzmann factor of the free energy change. The

next step in the method of Hwang and Warshel is to utilize a formula identical to Eq. (1.22) in this chapter to compute the free energy change. They employed an empirical valence bond (EVB) approach to approximately model electronic effects, and the calculations included the full experimental structure of carbonic anhydrase. An H/D isotope effect of 3.9 ± 1.0 was obtained in the calculation, which compared favorably with the experimental value of 3.8. This benchmark calculation gives optimism that quantum effects on free energies can be realistically modeled for complex biochemical systems.

Finally, related to the discussions of *ab initio* water above, enzyme reactions involve the making and breaking of chemical bonds. So classical forcefields are questionable for these problems. We can expect to see future research directed at *ab initio* simulation methods to handle those effects coupled with path integral or approximate quantum free energy methods to treat the nuclear quantum effects. These topics are broadly reviewed in Ref. [22].

- *Methods similar to those discussed in this chapter have been applied to determine free energies of activation in enzyme kinetics. They hold promise to be coupled with ab initio simulations to compute accurate estimates of nuclear quantum effects on rate constants in transition state theory.*

1.12 Summary

The list of fluids which exhibit important quantum effects is not large. Getting back to the original question of this chapter, it is clear that for liquids like helium and hydrogen, a full quantum treatment is necessary. Liquids such as neon and water, however, show modest quantum effects which can be modeled with approximate free energy methods. The quantum correction to the free energy of water is roughly 10% — this magnitude is large enough to warrant inclusion in calculations of free energies. As discussed in the introduction, there are experimentally observed isotope effects on solubilities of small nonpolar molecules and biomolecules, and protein stability.

The quasi-chemical calculations discussed above are a first major step towards determining the relative magnitudes of the various factors contributing to the excess chemical potential of water. The factors include packing effects, chemical contributions from local interactions, electrostatics, van der Waals interactions, molecular flexibility, electronic polarization, and quantum effects. *Ab initio* simulation methods, although computationally challenging, remove many of the uncertainties inherent in empirical forcefields. It appears that rigid water models better reproduce experimental structural properties than flexible models, but the origin of this observation is not entirely clear [38]. An alternative to the rigid model would be to compute an intramolecular potential of mean force from the ground state vibrational wavefunction of water and include this potential during classical propagation; this approach is consistent with the fact that it is easy to generate the exact intramolecular partition function q_{α}^{int} . Adding quantum effects for flexible water with

path integral calculations requires handling two very different energy-scale quantum effects on the same footing. But the *intermolecular* quantum effects are modest, and this chapter has discussed evidence that the QFH approach can handle those effects quite well. Thus, it would be interesting to see free energy computations performed using a combination of *ab initio* simulation along with the approximate quantum models. Establishing quantitative conclusions concerning the factors contributing to the excess chemical potential of water is a major challenge for molecular fluid free energy calculations. An even bigger challenge is extending the quantum mechanical methods discussed here to problems as complex as biomolecule solvation and enzyme kinetics.

At a practical level, what is the current status of methods for studying quantum effects on condensed phase free energies? If the quantum effects are relatively large, path integral methods are required. These techniques are mature, and the convergence of the calculations with increasing numbers of quantum degrees of freedom can easily be monitored. So long as an underlying classical interaction potential is employed, the additional computational cost is directly proportional to the number of variables needed to describe the paths. Thus, systems with hundreds of atoms can be handled on single workstations. The combination of path integral simulation with *ab initio* DFT methods is extremely challenging, however – systems with only tens of water molecules can be modeled for tens of ps. This is a frontier methods development problem for the computer simulation of liquids. Progress will involve both the further development of linear scaling algorithms for *ab initio* DFT and increased computer power. Improvements in DFT potentials should proceed in parallel with the development of more efficient numerical methods.

The effective potentials described in this chapter, on the other hand, are suited for relatively weak intermolecular quantum effects and require only a slight additional computational overhead – more terms in the potential – relative to routine classical simulations. Therefore, systems with tens of thousands of atoms can readily be modeled. This makes possible the large-scale simulation of biomolecule solvation with inclusion of quantum effects. If the intermolecular effective potentials ride atop a classical *ab initio* DFT simulation the overall cost should be comparable to the purely classical DFT modeling, but that approach has not been worked out yet.

To reiterate, a main obstacle to overcome is a useful partitioning of quantum effects into intra- and inter-molecular contributions during the *ab initio* simulation of molecular fluids with minor quantum effects. *Ab initio* simulation of a liquid like water is necessary to treat the complex charge redistribution effects and perhaps chemical reactions which may occur in the condensed phase. And quantum effects can't be entirely neglected since they have a significant magnitude. Therefore, development of new computational methods for this partitioning should open the door to the quantitative modeling of aqueous solutions and their interactions with biomolecules.

1.13 Acknowledgments

This research was supported by the National Science Foundation (CHE-0112322) and the DoD MURI program. I would like to especially thank Lawrence Pratt, Jim Doll, Rob Coalson, Dubravko Sabo, and Cristian Predescu for helpful discussions.

References

1. Feynman RP and Hibbs AR (1965) *Quantum Mechanics and Path Integrals*. McGraw-Hill, New York
2. Feynman RP (1972) *Statistical Mechanics*. Benjamin/Cummings, London
3. Chandler D and Wolynes PG (1981) *J Chem Phys* 74:4078–4095
4. Ceperley DM (1995) *Rev Mod Phys* 67:279–355
5. Parrinello M and Rahman A (1984) *J Chem Phys* 80:860–867
6. Laria D and Chandler D (1987) *J Chem Phys* 87:4088–4092
7. Marchi M, Sprik M, and Klein ML (1988) *J Phys Chem* 92:3625–3629
8. Wang Q, Johnson JK, and Broughton JQ (1996) *Mol Phys* 89:1105–1119
9. Wang Q, Johnson JK, and Broughton JQ (1997) *J Chem Phys* 107:5108–5117
10. Poulsen JA, Nyman G, and Rossky PJ (2004) *J Phys Chem B* 108:19799–19808
11. Sese LM (1992) *Molec Phys* 76:1335–1346
12. Tchouar N, Ould-Kaddur F, and Levesque D (2004) *J Chem Phys* 121:7326–7331
13. Thirumalai D, Hall RW, and Berne BJ (1984) *J Chem Phys* 81:2523–2527
14. Morales JJ and Singer K (1991) *Molec Phys* 73:873–880
15. Sese LM (1993) *Molec Phys* 78:1167–1177
16. Ortiz V and Lopez GE (2002) *Molec Phys* 100:1003–1009
17. Sese LM (1991) *Molec Phys* 74:177–189
18. T F Miller III and Clary DC (2003) *J Chem Phys* 119:68–76
19. Srinivisan J, Volobuev YL, Mielke SL, and Truhlar DG (2000) *Comput Phys Commun* 128:446–464
20. Doll JD, Beck TL, and Freeman DL (1990) *Adv Chem Phys* 78:61–127
21. Hwang JK and Warshel A (1996) *J Am Chem Soc* 118:11745–11751
22. Gao J and Truhlar DG (2002) *Ann Rev Phys Chem* 53:467–505
23. Runge KJ and Chester GV (1988) *Phys Rev B* 38:135–162
24. Barrat JL, Loubeyre P, and Klein ML (1989) *J Chem Phys* 90:5644–5650
25. Li D and Voth GA (1992) *J Chem Phys* 96:5340–5353
26. Liu A and Beck TL (1995) *Mol Phys* 86:225–233
27. Guillot B and Guissani Y (1998) *J Chem Phys* 108:10162–10174
28. Ben-Naim A and Marcus Y (1984) *J Chem Phys* 81:2016–2027
29. Gripon C, Legrand L, Rosenman I, Vidal O, Robert MC, and Boue F (1997) *J Cryst Growth* 177:238–247
30. Bonnete F, Madern D, and Zaccai G (1994) *J Molec Biol* 244:436–447
31. Beck TL, Paulaitis ME, and Pratt LR (2005) *The Potential Distribution Theorem and Models of Molecular Solutions*. Cambridge, New York. In press.
32. Mahoney MW and Jorgensen WL (2001) *J Chem Phys* 115:10758–10768
33. Chen B, Ivanov I, Klein ML, and Parrinello M (2003) *Phys Rev Letts* 91:215503

34. Asthagiri D, Pratt LR, and Kress JD (2003) *Phys Rev E* 68:041505
35. Fernandez-Serra MV, Ferlat G, and Artacho E (2004) Los Alamos Eprint archive: cond-mat/0407724
36. Kuo IFW, Mundy CJ, McGrath MJ, Siepmann JI, VandeVondele J, Sprik M, Hutter J, Chen B, Klein ML, Mohamed F, Krack M, and Parrinello M (2004) *J Phys Chem B* 108:12990–12998
37. Schwegler E, Grossman JC, Gygi F, and Galli G (2004) *J Chem Phys* 121:5400–5409
38. Allesch M, Schwegler E, Gygi F, and Galli G (2004) *J Chem Phys* 120:5192
39. Widom B (1963) *J Chem Phys* 39:2808–2812
40. Widom B (1982) *J Phys Chem* 86:869–872
41. Landau LD and Lifshitz EM (1980) *Statistical Physics*. Pergamon, New York, 3rd ed.
42. Stratt RM (1979) *J Chem Phys* 70:3630–3638
43. Kleinert H (1995) *Path Integrals in Quantum Mechanics, Statistics, and Polymer Physics*. World Scientific, Singapore
44. Coalson RD (1986) *J Chem Phys* 85:926
45. Pratt LR (1986) *J Chem Phys* 85:5045–5048
46. Beck TL (1992) *J Chem Phys* 96:7175–7177
47. Beck TL and Marchioro TL (1993) In Grabert H, Inomata A, Schulman L, and Weiss U (eds.) “Path Integrals from meV to MeV: Tutzing 1992,” 238–243. World Scientific, Singapore
48. van Kampen NG (1992) *Stochastic Processes in Physics and Chemistry*. Elsevier, New York
49. Jarzynski C (1997) *PhysRev Lett* 78:2690–2693
50. Roepstorff G (1994) *Path Integral Approach to Quantum Physics*. Springer-Verlag, New York
51. Predescu C (2003) *J Math Phys* 44:1226–1239
52. Lobaugh J and Voth GA (1997) *J Chem Phys* 106:2400–2410
53. de la Pena LH and Kusalik PG (2004) *J Chem Phys* 121:5992–6002
54. Stern HA and Berne BJ (2001) *J Chem Phys* 115:7622
55. Gray CG and Gubbins KE (1984) *Theory of Molecular Fluids. Volume 1: Fundamentals*. Oxford, Oxford
56. Predescu C and Doll JD (2003) *J Chem Phys* 117:7448–7463
57. Mielke SL and Truhlar DG (2001) *J Chem Phys* 114:621–630
58. Kuharski RA and Rosky PJ (1985) *J Chem Phys* 82:5164–5177
59. Wallqvist A and Berne BJ (1985) *Chem Phys Lett* 117:214
60. Goldman N, Leforestier C, and Saykally RJ (2005) *Phil Trans R Soc A* 1–16. Doi:10.1098/rsta.2004.1504
61. Sit P and Marzari N (2005) Los Alamos Eprint Server Cond-mat/0504146
62. de la Pena LH and Kusalik PG (2005) *J Am Chem Soc* 127:5246–5251
63. Grossman JC, Schwegler E, Draeger EW, Gygi F, and Galli G (2004) *J Chem Phys* 120:300–311
64. Lobaugh J and Voth GA (1996) *J Chem Phys* 104:2056–2069
65. Saam J, Tajkhorshid E, Hayashi S, and Schulten K (2002) *Biophys J* 83:3097–3112
66. Brewer ML, Schmitt UW, and Voth GA (2001) *Biophys J* 80:1691–1702
67. Wu Y and Voth GA (2003) *Biophys J* 85:864–875
68. Chakrabarti N, Roux B, and Pomes R (2004) *J Mol Biol* 343:493–510
69. Yin J, Kuang Z, Mahankali U, and Beck TL (2004) *Proteins: Struct, Funct, and Bioinform* 57:414–421